

Original Research

A Novel Automatic Real-time Motion Tracking Method for Magnetic Resonance Imaging-guided Radiotherapy: Leveraging the Enhanced Tracking-Learning-Detection Framework with Automatic Segmentation

Shengqi Chen¹;

Zilin Wang¹;

Jianrong Dai²;

Shirui Qin²;

Ying Cao²;

Ruiao Zhao²;

Jiayun Chen^{2*}; (Corresponding author, Email: grace_chenjy@163.com)

Guohua Wu^{1*}; (Corresponding author, Email: wuguohua@bupt.edu.cn)

Yuan Tang^{2*}; (Corresponding author, Email: tangyuan82@126.com)

* These authors contributed equally to this work. Jiayun Chen, Guohua Wu and Yuan Tang contributed equally as corresponding authors

¹ School of Electronic Engineering, Beijing University of Posts and Telecommunications, Beijing, China

² Department of Radiation Oncology, National Cancer Center/National Clinical Research Center for Cancer/Cancer Hospital, Chinese Academy of Medical Sciences and Peking Union Medical College, Beijing, China

【Abstract】

Background and Purpose: Accurate motion tracking in MRI-guided Radiotherapy (MRIgRT) is essential for effective treatment delivery. This study aimed to enhance motion tracking precision in MRIgRT through an automatic real-time markerless tracking method using an enhanced Tracking-Learning-Detection (ETLD) framework with automatic segmentation.

Materials and Methods: We developed a novel MRIgRT motion tracking and segmentation method by integrating the ETLD framework with an improved Chan-Vese model (ICV), named ETLD+ICV. The ETLD framework was upgraded for real-time cine MRI, including advanced image preprocessing, no-reference image quality assessment, an enhanced median-flow tracker, and a refined detector with dynamic search region adjustments. ICV was used for precise target volume coverage, refining the segmented region frame by frame using tracking results, with key parameters optimized. The method was tested on 3.5D MRI scans from 10 patients with liver metastases.

Results: Evaluation of 106,000 frames across 77 treatment fractions showed sub-millimeter tracking errors of less than 0.8mm, with over 99% precision and 98% recall for all subjects in the Beam Eye View(BEV)/Beam Path View(BPV) orientation. The ETLD+ICV method achieved a dice global score of more than 82% for all subjects, demonstrating the method's extensibility and precise target volume coverage.

Conclusion: This study successfully developed an automatic real-time markerless motion tracking method for MRIgRT that significantly outperforms current methods. The novel method not only delivers exceptional precision in tracking and segmentation but also shows enhanced adaptability to clinical demands, making it an indispensable asset in improving the efficacy of

radiotherapy treatments.

【 Key words 】 Real-time Tracking Method, Enhanced Tracking-Learning-Detection framework, Improved Chan-Vese model, MRIgRT, liver metastases

1. Introduction

Radiotherapy is a critical treatment in clinical oncology, efficiently targeting tumors while protecting surrounding healthy tissues. Nearly 70% of cancer patients undergo radiotherapy at some point^[1, 2], aiming to deliver concentrated radiation doses to the tumor volume while minimizing exposure to healthy tissues^[3, 4]. However, physiological processes like respiration and gastrointestinal activity can cause tumor position shifts of 2-14 mm, potentially compromising radiation delivery and increasing the dose to healthy tissues, thus affecting treatment efficacy^[3, 5, 6]. Studies show minor intra-fraction motion can significantly reduce radiation doses to the liver by up to 24%, and in the absence of motion adaptation, liver tumors can experience a dose reduction of over 29%^[7-9]. Accurate compensation for such shifts is essential to ensure the tumor receives the prescribed dose while minimizing effects on healthy tissues, making the management of intra-fraction motion a critical focus for enhancing patient outcomes^[6, 10].

Image-guided radiotherapy (IGRT) is a key strategy for precision radiotherapy, with cone-beam CT (CBCT) commonly used for tumor positioning verification^[2, 11]. However, CBCT has limitations, including extended scanning times and limited tissue contrast^[12]. Tumor surrogates like the diaphragm and chest wall have been used for tracking, but correlations can vary among

individuals^[13-15]. Invasive methods, such as implanting gold fiducials within tumors, introduce discomfort and uncertainties^[4, 16-18].

Magnetic resonance imaging-guided radiotherapy (MRIgRT) offers superior soft tissue contrast and real-time imaging, facilitating accurate tumor targeting and reducing radiation toxicity^[11, 19]. Despite early clinical adoption, MRIgRT has shown substantial benefits for cancer patients^[20, 21]. Accelerated imaging methods have made MRIgRT viable for online treatment plan adaptation, with MRI-Linacs providing comprehensive information throughout treatment, supporting both manual and automatic decision-making^[2, 19, 22, 23]. It is envisioned that MRIgRT will play a transformative role in IGRT.

In MRIgRT, physicians can dynamically adjust the planning target volume (PTV) during treatment^[19]. However, current systems often rely on manual contouring, which is inefficient and prone to inconsistencies^[24]. Imaging artifacts can also impair radiograph interpretation^[25].

To address these challenges, studies have investigated automatic, markerless motion management based on MRI, offering non-invasive benefits^[26-35]. Machine learning-based methods have been employed for motion estimation, but further refinement is needed for sub-millimeter accuracy. Some methods are not end-to-end, requiring additional steps^[26-29, 31, 33].

Deep learning, reliant on pre-trained models, faces challenges in applying to newly developed MRI imaging sequences due to requiring extensive datasets for training^[32, 34, 35]. The scarcity of available data limits the feasibility of deep learning, traditionally relying on large volumes of data to create robust, pre-trained models^[24]. Discrepancies between training and test sets can diminish accuracy, resulting in unpredictable performance when models are applied to new datasets. Inconsistencies in manually labeled ground truth can also impose constraints on the

deep learning training process^[4]. This limitation underscores the need for alternative or innovative methods that can adapt to limited data scenarios often encountered with novel imaging technologies.

In this study, we introduce an innovative tracking method designed to tackle real-time target motion management during MRIgRT. Our method is based on an enhanced Tracking-Learning-Detection algorithm^[36], adapted for high spatial and temporal resolution MRI imaging sequences, complemented by a proven automatic segmentation method. By integrating image pre-processing with a no-reference image quality assessment (NRIQA), our method achieves sub-millimeter tracking accuracy without pre-training. This advancement ensures precise tracking of target volumes and maintains high-accuracy standards for real-time applications. The efficacy of our proposed method is validated through rigorous testing on an MRI image dataset, demonstrating its potential to significantly enhance the precision and efficiency of MRIgRT procedures.

2. Materials and Methods

2.1. High Spatial and Temporal Resolution MRI Method with BEV/BPV Fusion Information

We've developed a 3.5D MRI technique that fuses BEV and BPV data, aligning the MRI centroid with the radiation beam's center^[2]. This technique creates three orthogonal planes: two BPV planes aligned with the radiation rays and one BEV plane perpendicular to them, all tailored to the tumor's centroid and radiation field orientation. It offers real-time localization of

the target volume and at-risk organs without needing post-processing adjustments.

2.2. Data Acquisition

Enrolled in a phase II clinical trial (NCT03927898), patients with colorectal cancer liver metastasis receiving MR-Linac Unity(Elekta AB, Stockholm, Sweden) treatment at our department from August 2021 to February 2024 provided informed consent for online MRgRT.

The treating radiation oncologist ensured there were no radiotherapy contraindications.

For 4D-CT scanning(Siemens Healthcare, Erlangen, Germany), patients were positioned supine with arms raised and supported (Siemens Healthcare). Target volumes were outlined, and IMRT plans were created using Monaco Version 5.4 (Elekta AB) with 6-9 beams. Abdominal compression belts restrict abdominal movement(RAM) during treatment, and 2D cine MR imaging tracked tumor positions for dose accuracy. After each treatment, the abdominal compression belt was reapplied to restrict abdominal movement, and 3.5D MRI data (group RAM) was acquired. Subsequently, patients were scanned in a free-breathing state to obtain 3.5D MRI data (group FB).

The study included data from 10 patients, with 3.5D MRI images captured across one BEV and two BPV planes at the isocenter, with 50 frames per plane at 4.347 Hz. A dataset of 112,800 frames from 77 fractions was compiled from 2D cine MRI images, providing a robust basis for tracking analysis.

2.3. Data Preprocessing

The spatial resolution and signal-to-noise ratio (SNR) of the patient data acquired through 3.5D MRI did not match the levels seen in natural images. To enhance image quality for TLD tracking

assumptions, we applied grayscale normalization, gamma correction, and Gaussian filtering. After testing 23 different preprocessing methods, we selected the final scheme based on its performance in the no-reference image quality assessment (section 2.4).

2.4. No Reference Image Quality Assessment (NRIQA)

The NRIQA method called 'BRISQUE' offers a vital solution in medical imaging, especially where high-quality reference images are unavailable, as it does not require comparative training data^[37]. Building on this, we utilized absolute deviation (MAD) weighting to dynamically assess image quality, meeting clinical needs and opening new avenues in image processing.

Our NRIQA analysis pinpointed the best preprocessing scheme by choosing the one with the top average quality score, as outlined in Section 2.3. To maintain data effectiveness, an admission mechanism filters out MRI data below the 5th percentile threshold, empirically determined by a radiation oncologist for optimal data quality and efficiency.

2.5. Enhanced Tracking-Learning-Detection (ETLD)

The original Tracking-Learning-Detection (OTLD) framework, a machine learning algorithm adept at long-term tracking of a single target within video streams^[36], has been meticulously refined for our study. This improved version termed the Enhanced Tracking-Learning-Detection (ETLD) method includes key improvements for real-time MRI-guided tracking.

The ETLD retains the core OTLD modules: an inter-frame motion tracker, a detector for exploring potential target locations, and a learning module that dynamically updates the detector's capabilities. As shown in Figure 1, it contains 4 stages, where the pre-processed cine-MRIs are processed through tracking, detection, learning, and integration into a single location

prediction. The enhancements are as follows:

- 1) Image Preprocessing: Images are preprocessed to optimize the tracker's performance, as detailed in sections 2.3 and 2.4.
- 2) Search Process Optimization: Considering that typical targets to be tracked are usually small and their sizes usually do not change significantly. We adjusted the window scanning size and image patch normalization to better accommodate small targets and refined the sliding window scaling factor from 1.2 to 1.1 to better search for potential target locations.
- 3) Median-Flow Tracker Enhancement: We enhanced the tracker's accuracy for small targets by reducing pyramid levels to 3 and expanding the Lucas-Kanade algorithm's neighborhood size to 31 pixels, along with increasing the iteration count.
- 4) Dynamic Search Region Adjustment: Based on liver tumor displacement data^[2], we confined the search region to a 30×30 -pixel area centered on the target's centroid from the last three frames, reducing false positives and enhancing tracking accuracy and efficiency.

2.6. Automatic Segmentation Process

The segmentation process has been refined for accurate radiotherapy beam coverage of the region of interest (ROI) by integrating the ETLD method with the Chan-Vese model^[38], a technique renowned for its iterative energy minimization in medical image segmentation^[39]. Specifically, the Chan-Vese model receives an MRI sequence and the initial target bounding box and is complemented by the ETLD's output for dynamic frame-by-frame refinements. This synergistic approach facilitates an automatic segmentation process that precisely monitors the target's morphological and positional variations throughout treatment. With optimized parameters, the ETLD+ICV method enhances precision in radiotherapy beam targeting and

improves segmentation efficiency for clinical reliability.

2.7. Evaluation Procedure

Our proposed method, implemented in C++ and MATLAB, and optimized for real-time location prediction through online learning, eliminates the need for pre-training and runs efficiently on a personal computer (PC) with an Intel(R) Core(TM) i9-13980HX processor and 32GB RAM, without GPU acceleration. It was tested in a Windows 11 environment with Visual Studio 2019 and OpenCV 3.3.1.

Due to the challenges in 3.5D MRI tumor delineation, blood vessels were tracked as a proxy for tumor motion, supported by a strong correlation between them^[40, 41]. The method was evaluated using data from 10 patients, amounting to 112,800 frames.

For rigorous evaluation, radiation oncologists manually created binary masks of tumor regions based on liver tumor motion, which were then verified twice for accuracy. Over 9 months, low-quality images were excluded, resulting in a refined dataset of 2,120 high-quality datasets and 106,000 frames.

2.8. Evaluation Metrics

The performance of the proposed method is rigorously evaluated using specific metrics:

2.8.1. Tracking Performance Evaluation

Precision in following the tumor center's trajectory by the radiation beam is crucial in clinical settings. Reflecting this priority, the real-time trajectory of the radiotherapy beam was simulated using the tracking algorithm's output. The mean absolute error (MAE), as shown in Equation

(1), is the primary metric for this assessment:

$$MAE = \frac{1}{N} \sum_{i=1}^N |\vec{P}_i - \vec{G}_i| \quad (1)$$

Here, \vec{P}_i and \vec{G}_i represent the predicted and actual displacement vectors at frame i , respectively, with $|\cdot|$ signifying the absolute value and N is the total number of frames. The MAE quantifies the tracking algorithm's adherence to the tumor's motion.

Additionally, the correlation coefficient (CC) was used to further validate tracking efficacy, with higher CC values indicating better performance^[42]. Precision and recall rates were also calculated across the dataset to evaluate clinical applicability.

2.8.2. Segmentation Performance Evaluation

For segmentation, the Dice coefficient, a standard metric, is used as shown in Equation (2):

$$Dice = \frac{2|mask_i^{prediction} \cap mask_i^{groundtruth}|}{|mask_i^{prediction}| + |mask_i^{groundtruth}|} \quad (2)$$

Here, $mask_i^{prediction}$ and $mask_i^{groundtruth}$ denote the predicted and actual segmentation masks, respectively, with \cap representing the intersection and $|\cdot|$ quantifies the pixel count.

Given the varying target sizes and the Dice coefficient's sensitivity^[43], the Dice global metric from the Liver Tumor Segmentation Challenge (LiTS)^[44] was applied to assess segmentation efficacy, capturing performance across varying target sizes and contour estimation sensitivity.

2.8.3. Computational Efficiency Evaluation

The frames per second (FPS) metric encapsulates the method's real-time capabilities. Tracking and segmentation FPS were calculated for each patient, and an average was derived to present the computational efficiency of the method, ensuring compliance with real-time clinical

radiotherapy constraints.

3. Results

3.1. Accuracy of motion estimation

Figure 2 displays the ETLD's tracking performance for a patient in the RAM group at a 140-degree gantry angle, with the red line representing the actual trajectory and the blue line the algorithm's predictions. The images highlight the close match between predictions and ground truth, indicating a strong correlation.

Figure 3 and Table 1 compare the ETLD and OTLD methods' tracking performance. The MAE box plot shows the ETLD's tracking errors mostly within a 1 mm threshold, with over 99% precision and 98% recall, while the OTLD underperforms in these metrics. Table 1 shows the ETLD achieved an MAE below 0.8 mm and a CC above 94% for all patients. Overall, ETLD's MAE was below 0.65 mm and CC above 96%, outperforming OTLD, which had an overall precision below 96%, recall below 77%, and CC below 95%.

A one-pass evaluation across varying location error thresholds, known as the precision plot^[45], was used to assess the algorithm's precision, along with a recall plot (Figure 4). This analysis shows the ETLD's ability to track a broader range of targets at different error thresholds compared to the OTLD. A location error threshold of 20 was selected to determine the precision and recall rates, as demonstrated in Figure 3 and Table 1.

3.2. Accuracy of Target Segmentation

Given the ETLD's superior tracking performance over OTLD, the OTLD+ICV combination

was not pursued. Figure 5 shows the segmentation performance of the ETLD+ICV method. Figure 5(a) displays a sample patient's segmentation results with ground truth in red and predictions in blue, revealing a high congruence with the ground truth, highlighting the algorithm's accuracy. Figure 5(b) summarizes the segmentation outcomes, with dice global values consistently above 82%. The mean dice global value of 87.7% confirms the effectiveness of the automatic segmentation method in precisely delineating target volumes.

3.3. Computational Efficiency of Tracking and Segmentation

The experiments, executed as detailed in Section 2.7, showed that our method achieved a mean processing frame rate of 22.304 ± 7.733 FPS for tracking and 25.180 ± 16.116 FPS for segmentation without GPU acceleration. On average, tracking took under 50 ms and segmentation below 40 ms per frame, despite patient variability. These results underscore the method's high efficiency, with total processing times not exceeding 100 milliseconds per frame, making it suitable for real-time radiotherapy applications.

4. Discussion

MRIgRT excels in precision radiotherapy by providing superior soft tissue contrast and avoiding the need for marker implantation^[19]. To enhance the accuracy of target volume motion estimation, we've developed a comprehensive tracking method. This method, supported by the TLD framework^[36], merges tracking and detection, improving its precision and response to target variations. It also includes a Chan-Vese model-based segmentation module for precise target segmentation.

The OTLD algorithm, known for its high-performance tracking, has been effectively used for

MRI target tracking^[33]. However, it encountered challenges with tracking failures and inaccuracies due to varying image quality between natural and MRI images, a common issue in MRIgRT motion management. To address the stringent precision requirements in radiotherapy, we developed the ETLD by enhancing the OTLD algorithm. Enhancements included image preprocessing, search process optimization, dynamic search region adjustment, and an enhanced median-flow tracker. To mitigate image quality biases, experiments utilized MRI data from higher magnetic field strengths (1.5T) and implemented a mechanism to filter out low-quality data.

Additionally, since the OTLD algorithm only provides location predictions, we integrated the Chan-Vese segmentation method with the ETLD to ensure precise ROI coverage. This innovative approach combines tracking and segmentation, overcoming the limitations of focusing solely on one aspect. Our method's tracking capabilities were validated with a 3.5D MRI dataset comprising 106,000 frames across 77 fractions. The results showed an average MAE of less than 0.8 mm, a CC exceeding 94.3%, and precision and recall rates surpassing 98% for all patients. In contrast, the OTLD method exhibited higher tracking errors and lower overall recall and precision rates.

Compared to previous studies, our method excels with a larger dataset and a tracking latency of under 50 ms, well below the "real-time" threshold of 500 ms defined by the AAPM Task Group 264^[46]. The ETLD+ICV method achieved a dice global score over 82%, averaging 87.7%, with processing times under 40 ms, comparable to U-net model results in MRI segmentation^[32], and was achieved without powerful GPUs, suggesting cost-effectiveness.

Real-time MRI-guided radiotherapy is emerging, with early studies like those by Yun J et al.

using pulse-coupled neural networks (PCNN) for lung tumor tracking within 3.5 mm errors, though requiring extensive pre-training^[26, 27]. Other methods, such as multi-template matching (MTM) and deformable image registration (DIR), have shown superior performance to PCNN^[31]. Bourque AE's team achieved millimeter-level accuracy with particle filters on 1.5T MRI images^[28, 29], but noted limitations with out-of-plane motion, a challenge also raised by Seregni M et al^[30]. Our method has proven robust against such issues. Deep learning models, including deep convolutional neural networks (DCNN) and improved U-net models, have shown potential in motion estimation^[34, 35], but rely on large-scale datasets for pre-training, leading to concerns about waiting times and generalization.

The studies discussed earlier partially uncover the challenges and limitations of MRI-based markerless motion management. Our method offers clear benefits due to the OTLD framework's online updating of the detector and object model, which effectively addresses out-of-plane motion effects like disappearances and deformations. The median-flow tracker guarantees consistent and accurate trajectory prediction. However, algorithm optimization remains crucial, with performance improvements evident in Table 1. The method's versatility is further demonstrated by its integration with the Chan-Vese model.

The proposed method accepts any sequence of continuous 2D images without pre-training, making it versatile across imaging modalities. It extends beyond MRI-Linacs to applications like intraoperative radiotherapy and ultrasound-guided biopsies, especially in proton therapy.

Proton therapy's challenges include daily imaging guidance issues: (i) visibility of many tumors, (ii) real-time tracking of moving tumors during dose delivery, and (iii) anatomical variation and organ movement. Combining MRI imaging with proton therapy promises precise and effective

dose implementation. Our ETLD+ICV tracking method stands out as a preferred solution for proton therapy's targeting accuracy in moving soft-tissue tumors.

Our method was tested on a 1.5T MRI dataset, but its robustness across different imaging qualities, such as 0.35T MRI, requires further confirmation. The absence of standardized datasets, due to varying equipment and protocols, complicates algorithm comparisons and accentuates the need for publicly available datasets. Future work will incorporate novel architectures such as the Region Proposal Network (RPN)^[47] to enhance tracking accuracy and efficiency. Additionally, performance validation in lower-quality data and quantitative evaluation of the proposed method's impact on clinical treatment outcomes remain necessary. Furthermore, potentially applying the method to other imaging scenarios like infrared scenes, will expand its applicability.

5. Conclusion

This study successfully developed and validated an automatic real-time markerless motion tracking method using the ETLD+ICV for MRIgRT. The method's high precision and recall rates, achieved without pre-training, surpass current techniques and offer significant improvements for MRIgRT, thereby enhancing radiotherapy effectiveness. The implications for radiotherapy are that advanced tracking systems may improve patient outcomes. Future studies will investigate further enhancements to the tracking algorithm and explore its application in other imaging contexts.

References:

- [1] XIA C, DONG X, LI H, et al. Cancer statistics in China and United States, 2022: profiles, trends,

- and determinants [J]. *Chin Med J (Engl)*, 2022, 135(5): 584-90.<https://doi.org/10.1097/CM9.0000000000002108>
- [2] JIAYUN C, XIAOQI W, SHIRUI Q, et al. A Novel High-resolution Fast Magnetic Resonance Imaging Method Incorporating BEV/BPV Fusion Information [J]. *Nuclear Physics Review*, 2024, 41(1): 1-6.<https://doi.org/10.11804/NuclPhysRev.41.2023CNPC72>
- [3] BERTHOLET J, KNOPF A, EIBEN B, et al. Real-time intrafraction motion monitoring in external beam radiotherapy [J]. *Phys Med Biol*, 2019, 64(15): 15TR01.<https://doi.org/10.1088/1361-6560/ab2ba8>
- [4] LIU X, GENG L S, HUANG D, et al. Deep learning-based target tracking with X-ray images for radiotherapy: a narrative review [J]. *Quant Imaging Med Surg*, 2024, 14(3): 2671-92.<https://doi.org/10.21037/qims-23-1489>
- [5] FAST M F, CAO M, PARIKH P, et al. Intrafraction Motion Management With MR-Guided Radiation Therapy [J]. *Semin Radiat Oncol*, 2024, 34(1): 92-106.<https://doi.org/10.1016/j.semradonc.2023.10.008>
- [6] WU V W C, NG A P L, CHEUNG E K W. Intrafractional motion management in external beam radiotherapy [J]. *J Xray Sci Technol*, 2019, 27(6): 1071-86.<https://doi.org/10.3233/XST-180472>
- [7] POULSEN P R, WORM E S, HANSEN R, et al. Respiratory gating based on internal electromagnetic motion monitoring during stereotactic liver radiation therapy: First results [J]. *Acta Oncol*, 2015, 54(9): 1445-52.<https://doi.org/10.3109/0284186X.2015.1062134>
- [8] NANKALI S, WORM E S, HANSEN R, et al. Geometric and dosimetric comparison of four intrafraction motion adaptation strategies for stereotactic liver radiotherapy [J]. *Phys Med Biol*, 2018, 63(14): 145010.<https://doi.org/10.1088/1361-6560/aacdda>
- [9] GIERGA D P, CHEN G T, KUNG J H, et al. Quantification of respiration-induced abdominal tumor motion and its impact on IMRT dose distributions [J]. *Int J Radiat Oncol Biol Phys*, 2004, 58(5): 1584-95.<https://doi.org/10.1016/j.ijrobp.2003.09.077>
- [10] WITT J S, ROSENBERG S A, BASSETTI M F. MRI-guided adaptive radiotherapy for liver tumours: visualising the future [J]. *Lancet Oncol*, 2020, 21(2): e74-e82.[https://doi.org/10.1016/S1470-2045\(20\)30034-6](https://doi.org/10.1016/S1470-2045(20)30034-6)
- [11] GREGOIRE V, GUCKENBERGER M, HAUSTERMANS K, et al. Image guidance in radiation therapy for better cure of cancer [J]. *Mol Oncol*, 2020, 14(7): 1470-91.<https://doi.org/10.1002/1878-0261.12751>
- [12] DHONT J, HARDEN S V, CHEE L Y S, et al. Image-guided Radiotherapy to Manage Respiratory Motion: Lung and Liver [J]. *Clin Oncol (R Coll Radiol)*, 2020, 32(12): 792-804.<https://doi.org/10.1016/j.clon.2020.09.008>
- [13] EDMUNDS D, SHARP G, WINEY B. Automatic diaphragm segmentation for real-time lung tumor tracking on cone-beam CT projections: a convolutional neural network approach [J]. *Biomed Phys Eng Express*, 2019, 5(3).<https://doi.org/10.1088/2057-1976/ab0734>
- [14] WEI J, CHAO M. A constrained linear regression optimization algorithm for diaphragm motion tracking with cone beam CT projections [J]. *Phys Med*, 2018, 46: 7-15.<https://doi.org/10.1016/j.ejmp.2018.01.005>
- [15] CERVIÑO L I, CHAO A K, SANDHU A, et al. The diaphragm as an anatomic surrogate for lung tumor motion [J]. *Physics in Medicine & Biology*, 2009, 54(11): 3529.<https://doi.org/10.1088/0031-9155/54/11/017>
- [16] MYLONAS A, KEALL P J, BOOTH J T, et al. A deep learning framework for automatic detection of

- arbitrarily shaped fiducial markers in intrafraction fluoroscopic images [J]. *Med Phys*, 2019, 46(5): 2286-97. <https://doi.org/10.1002/mp.13519>
- [17] LIANG Z, ZHOU Q, YANG J, et al. Artificial intelligence-based framework in evaluating intrafraction motion for liver cancer robotic stereotactic body radiation therapy with fiducial tracking [J]. *Med Phys*, 2020, 47(11): 5482-9. <https://doi.org/10.1002/mp.14501>
- [18] BHAGAT N, FIDELMAN N, DURACK J C, et al. Complications associated with the percutaneous insertion of fiducial markers in the thorax [J]. *Cardiovasc Intervent Radiol*, 2010, 33(6): 1186-91. <https://doi.org/10.1007/s00270-010-9949-0>
- [19] KEALL P J, BRIGHI C, GLIDE-HURST C, et al. Integrated MRI-guided radiotherapy - opportunities and challenges [J]. *Nat Rev Clin Oncol*, 2022, 19(7): 458-70. <https://doi.org/10.1038/s41571-022-00631-3>
- [20] VAN DAMS R, WU T C, KISHAN A U, et al. Ablative radiotherapy for liver tumors using stereotactic MRI-guidance: A prospective phase I trial [J]. *Radiother Oncol*, 2022, 170: 14-20. <https://doi.org/10.1016/j.radonc.2021.06.005>
- [21] FINAZZI T, HAASBEEK C J A, SPOELSTRA F O B, et al. Clinical Outcomes of Stereotactic MR-Guided Adaptive Radiation Therapy for High-Risk Lung Tumors [J]. *Int J Radiat Oncol Biol Phys*, 2020, 107(2): 270-8. <https://doi.org/10.1016/j.ijrobp.2020.02.025>
- [22] GAO Y, ZHOU Z, HAN F, et al. Accelerated 3D bSSFP imaging for treatment planning on an MRI-guided radiotherapy system [J]. *Med Phys*, 2018, 45(6): 2595-602. <https://doi.org/10.1002/mp.12924>
- [23] BRUIJNEN T, STEMKENS B, LAGENDIJK J J W, et al. Multiresolution radial MRI to reduce IDLE time in pre-beam imaging on an MR-Linac (MR-RIDDLE) [J]. *Phys Med Biol*, 2019, 64(5): 055011. <https://doi.org/10.1088/1361-6560/aafd6b>
- [24] ZHOU S K, GREENSPAN H, DAVATZIKOS C, et al. A review of deep learning in medical imaging: Imaging traits, technology trends, case studies with progress highlights, and future promises [J]. *Proc IEEE Inst Electr Electron Eng*, 2021, 109(5): 820-38. <https://doi.org/10.1109/JPROC.2021.3054390>
- [25] HAVSTEEN I, OHLHUES A, MADSEN K H, et al. Are Movement Artifacts in Magnetic Resonance Imaging a Real Problem?-A Narrative Review [J]. *Front Neurol*, 2017, 8: 232. <https://doi.org/10.3389/fneur.2017.00232>
- [26] YUN J, YIP E, GABOS Z, et al. Neural-network based autocontouring algorithm for intrafractional lung-tumor tracking using Linac-MR [J]. *Med Phys*, 2015, 42(5): 2296-310. <https://doi.org/10.1118/1.4916657>
- [27] YUN J, YIP E, GABOS Z, et al. Improved lung tumor autocontouring algorithm for intrafractional tumor tracking using 0.5 T linac-MR [J]. *Biomedical Physics & Engineering Express*, 2016, 2(6). <https://doi.org/10.1088/2057-1976/2/6/067004>
- [28] BOURQUE A E, CARRIER J-F, FILION É, et al. A particle filter motion prediction algorithm based on an autoregressive model for real-time MRI-guided radiotherapy of lung cancer [J]. *Biomedical Physics & Engineering Express*, 2017, 3(3). <https://doi.org/10.1088/2057-1976/aa6b5b>
- [29] BOURQUE A E, BEDWANI S, CARRIER J F, et al. Particle Filter-Based Target Tracking Algorithm for Magnetic Resonance-Guided Respiratory Compensation: Robustness and Accuracy Assessment [J]. *Int J Radiat Oncol Biol Phys*, 2018, 100(2): 325-34. <https://doi.org/10.1016/j.ijrobp.2017.10.004>

- [30] SEREGNI M, PAGANELLI C, SUMMERS P, et al. A Hybrid Image Registration and Matching Framework for Real-Time Motion Tracking in MRI-Guided Radiotherapy [J]. IEEE Trans Biomed Eng, 2018, 65(1): 131-9.<https://doi.org/10.1109/TBME.2017.2696361>
- [31] FAST M F, EIBEN B, MENTEN M J, et al. Tumour auto-contouring on 2d cine MRI for locally advanced lung cancer: A comparative study [J]. Radiother Oncol, 2017, 125(3): 485-91.<https://doi.org/10.1016/j.radonc.2017.09.013>
- [32] FRIEDRICH F, HORNER-RIEBER J, RENKAMP C K, et al. Stability of conventional and machine learning-based tumor auto-segmentation techniques using undersampled dynamic radial bSSFP acquisitions on a 0.35 T hybrid MR-linac system [J]. Med Phys, 2021, 48(2): 587-96.<https://doi.org/10.1002/mp.14659>
- [33] DHONT J, VANDEMEULEBROUCKE J, CUSUMANO D, et al. Multi-object tracking in MRI-guided radiotherapy using the tracking-learning-detection framework [J]. Radiother Oncol, 2019, 138: 25-9.<https://doi.org/10.1016/j.radonc.2019.05.008>
- [34] TERPSTRA M L, MASPERO M, BRUIJNEN T, et al. Real-time 3D motion estimation from undersampled MRI using multi-resolution neural networks [J]. Med Phys, 2021, 48(11): 6597-613.<https://doi.org/10.1002/mp.15217>
- [35] SHAO H C, LI T, DOHOPOLSKI M J, et al. Real-time MRI motion estimation through an unsupervised k-space-driven deformable registration network (KS-RegNet) [J]. Phys Med Biol, 2022, 67(13): 135012.<https://doi.org/10.1088/1361-6560/ac762c>
- [36] KALAL Z, MIKOLAJCZYK K, MATAS J. Tracking-Learning-Detection [J]. IEEE Trans Pattern Anal Mach Intell, 2012, 34(7): 1409-22.<https://doi.org/10.1109/TPAMI.2011.239>
- [37] MITTAL A, MOORTHY A K, BOVIK A C. No-reference image quality assessment in the spatial domain [J]. IEEE Trans Image Process, 2012, 21(12): 4695-708.<https://doi.org/10.1109/TIP.2012.2214050>
- [38] CHAN T F, VESE L A. Active contours without edges [J]. IEEE Trans Image Process, 2001, 10(2): 266-77.<https://doi.org/10.1109/83.902291>
- [39] LEWIS B, GUTA A, SHIN J, et al. Evaluating motion of pancreatic tumors and anatomical surrogates using cine MRI in 0.35T MRgRT under free breathing conditions [J]. J Appl Clin Med Phys, 2023, 24(6): e13930.<https://doi.org/10.1002/acm2.13930>
- [40] JUPITZ S A, SHEPARD A J, HILL P M, et al. Investigation of tumor and vessel motion correlation in the liver [J]. J Appl Clin Med Phys, 2020, 21(8): 183-90.<https://doi.org/10.1002/acm2.12943>
- [41] ROSENBERG S A, HENKE L E, SHAVERDIAN N, et al. A Multi-Institutional Experience of MR-Guided Liver Stereotactic Body Radiation Therapy [J]. Adv Radiat Oncol, 2019, 4(1): 142-9.<https://doi.org/10.1016/j.adro.2018.08.005>
- [42] GRAMA D, DAHELE M, VAN ROOIJ W, et al. Deep learning-based markerless lung tumor tracking in stereotactic radiotherapy using Siamese networks [J]. Med Phys, 2023, 50(11): 6881-93.<https://doi.org/10.1002/mp.16470>
- [43] WEI R, CHEN J, LIANG B, et al. Real-time 3D MRI reconstruction from cine-MRI using unsupervised network in MRI-guided radiotherapy for liver cancer [J]. Med Phys, 2023, 50(6): 3584-96.<https://doi.org/10.1002/mp.16141>
- [44] BILIC P, CHRIST P, LI H B, et al. The Liver Tumor Segmentation Benchmark (LiTS) [J]. Med Image Anal, 2023, 84: 102680.<https://doi.org/10.1016/j.media.2022.102680>
- [45] WU Y, LIM J, YANG M H. Online Object Tracking: A Benchmark; proceedings of the 2013 IEEE Conference on Computer Vision and Pattern Recognition, F 23-28 June 2013, 2013

[C].<https://doi.org/10.1109/CVPR.2013.312>

- [46] KEALL P J, SAWANT A, BERBECO R I, et al. AAPM Task Group 264: The safe clinical implementation of MLC tracking in radiotherapy [J]. Med Phys, 2021, 48(5): e44-e64.<https://doi.org/10.1002/mp.14625>
- [47] REN S, HE K, GIRSHICK R, et al. Faster R-CNN: Towards Real-Time Object Detection with Region Proposal Networks [J]. IEEE Trans Pattern Anal Mach Intell, 2017, 39(6): 1137-49.<https://doi.org/10.1109/TPAMI.2016.2577031>

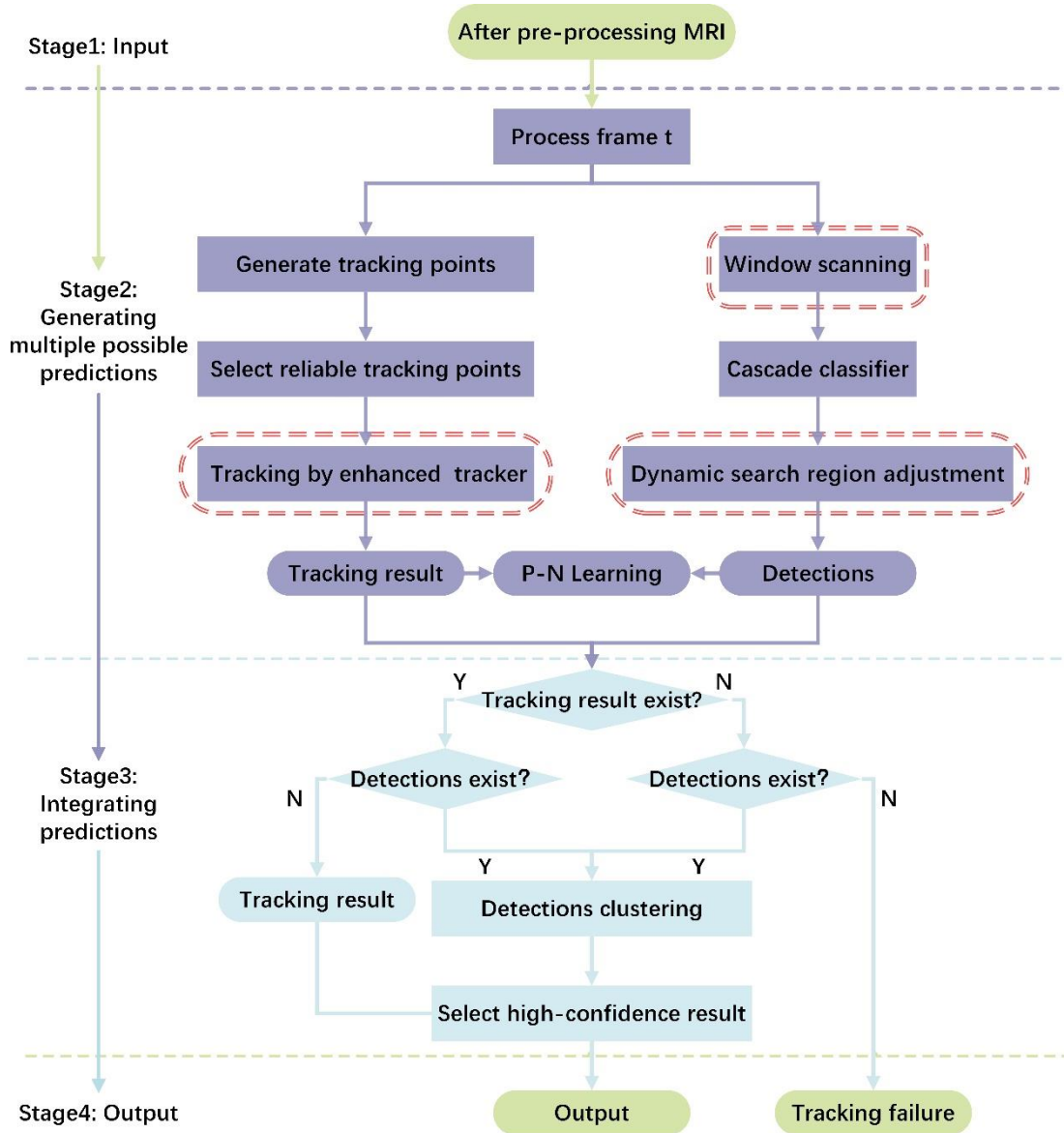


Figure 1. The main workflow of the ETLD method. The red rounded rectangles denote the main improvements based on the OTLD.

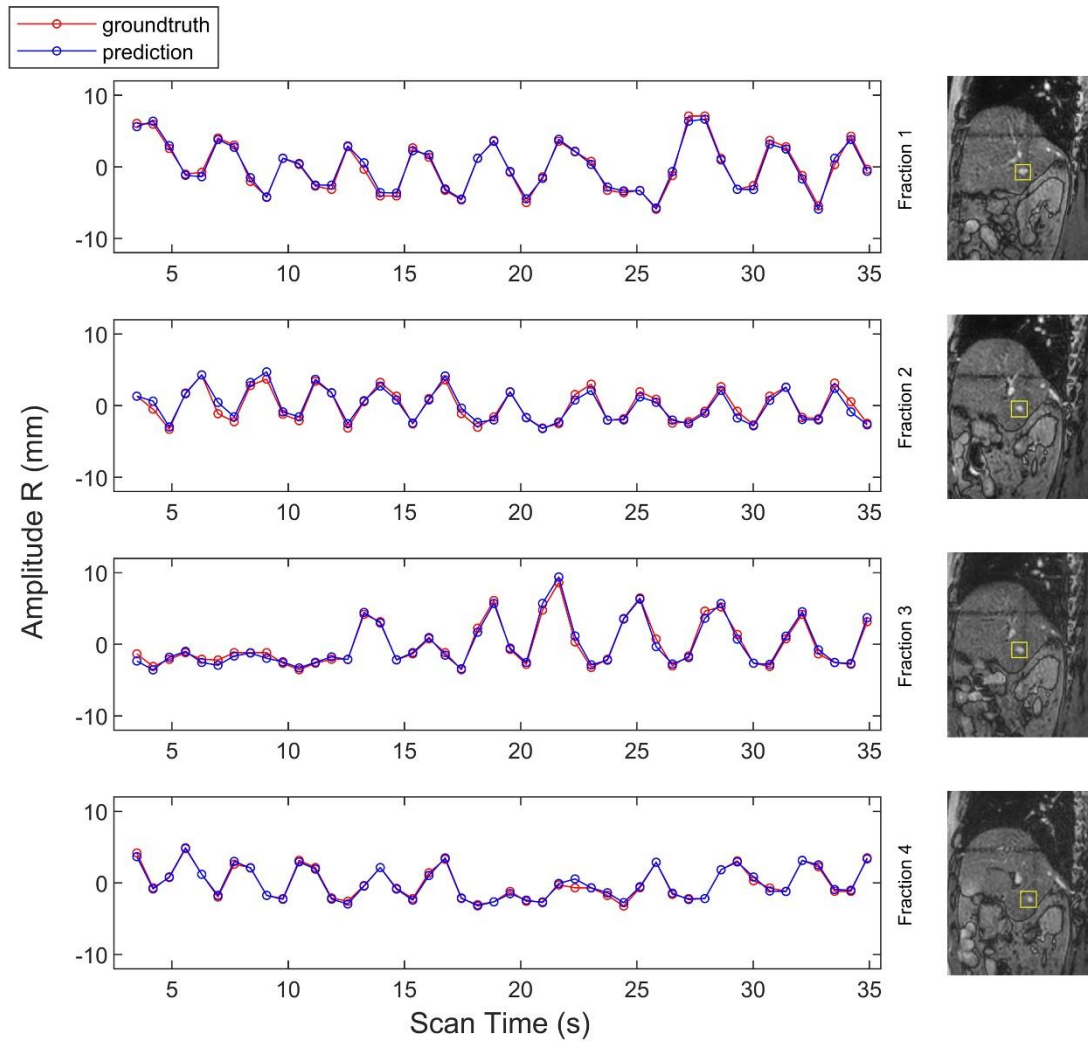


Figure 2. The tracking results of the ETLD on patient 1's data within the RAM group at a 140-degree angle. The graph juxtaposes the actual tumor displacement (red line) with the predicted tracking (blue line), demonstrating the close correlation between the two. Accompanying images showcase the precision of tracking in representative frames, with minimal divergence between the ground truth and predictions, indicative of the algorithm's high fidelity in motion estimation.

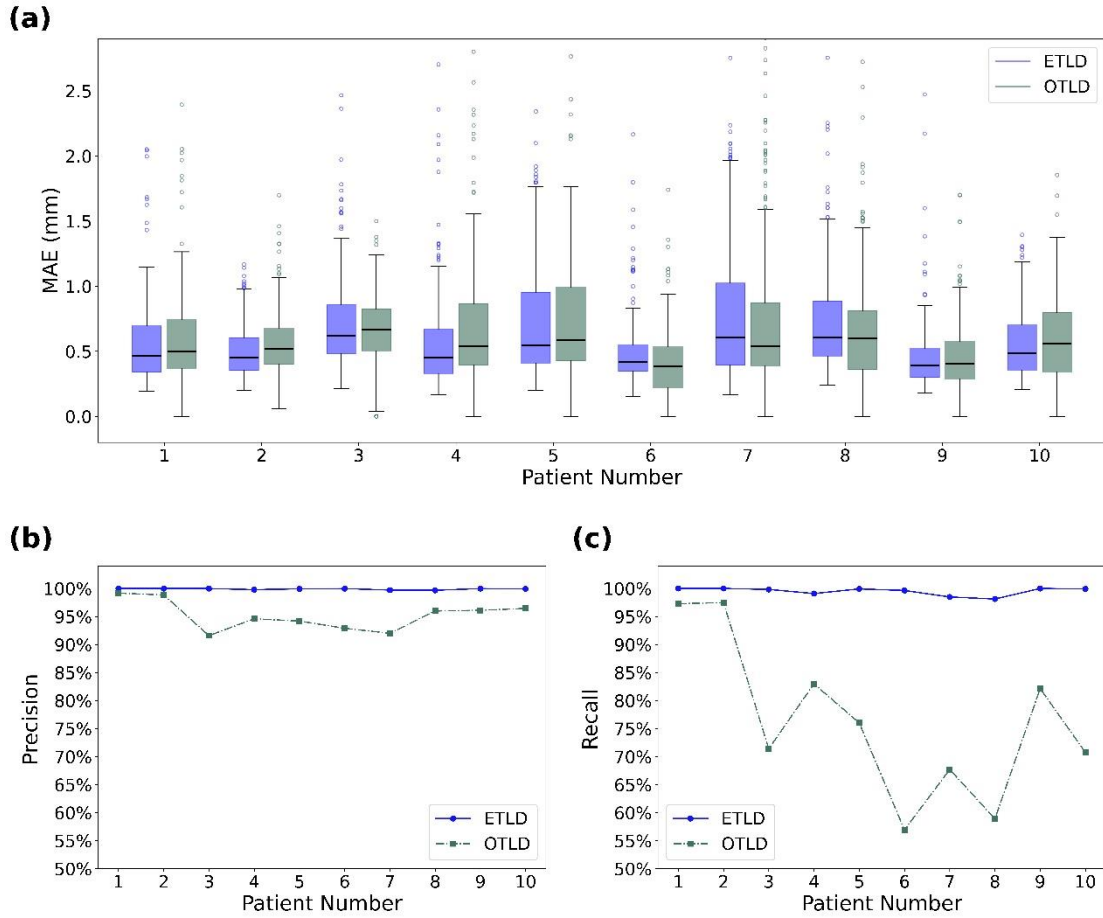


Figure 3. Comparative tracking performance evaluation of the ETLD and the OTLD methods across multiple patients (n=10). (a) The box plot of the MAE in tracking accuracy. (b) The line plot of the precision in tracking. (c) The line plot of the recall in tracking.

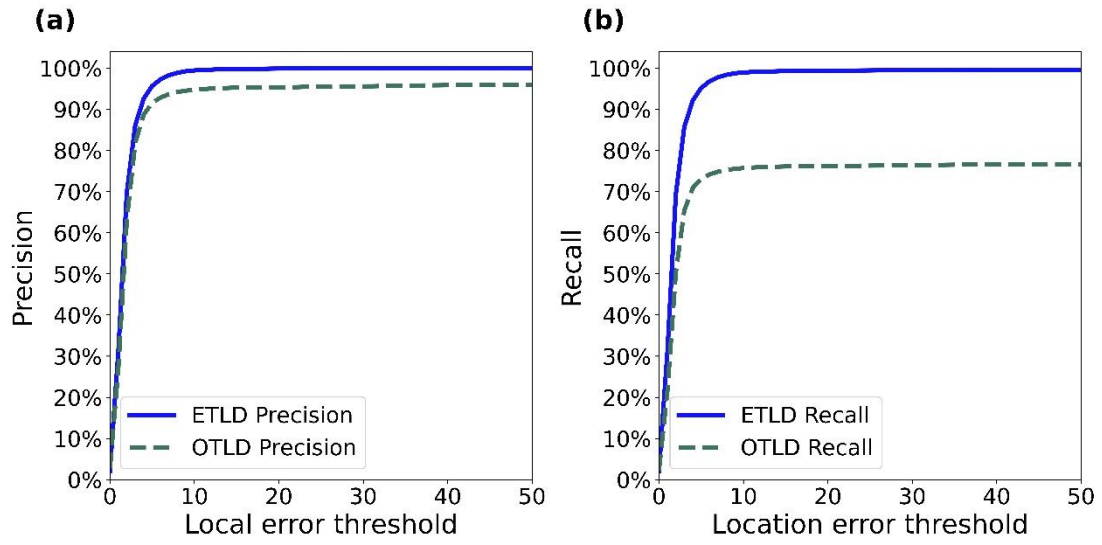


Figure 4. The precision and recall plot of the ETLD and OTLD methods. (a) The precision plot. (b) The recall plot.

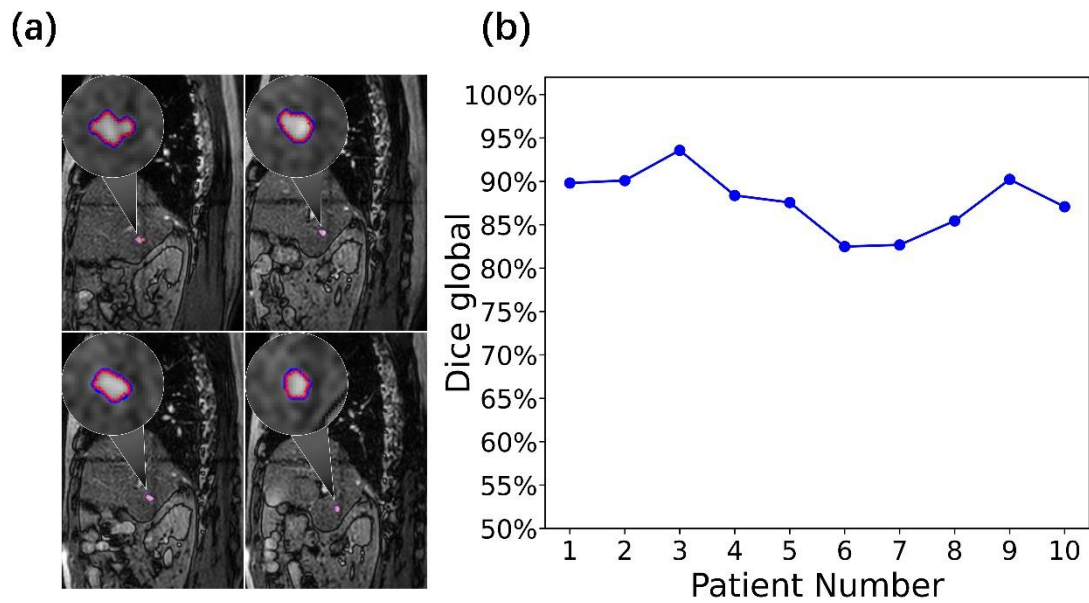


Figure 5. Segmentation accuracy assessment of the ETLD+ICV method. (a) Direct comparison of segmentation masks for a sample patient, with ground truth in red and predictions in blue. (b) Compilation of dice global values, evidencing the segmentation accuracy across all test patients (n=10).

NOTE. In Figure 5(a), the circular region represents the magnified view, with a magnification factor of 4.

Table 1. Comparative analysis of tracking performance metrics between the ETLD and OTLD algorithms across multiple patients (n=10). The table displays MAE in millimeters, CC, precision, and recall rates for each patient and the aggregate data.

Patient	MAE (mm)		CC		Precision		Recall	
	ETLD	OTLD	ETLD	OTLD	ETLD	OTLD	ETLD	OTLD
1	0.602±0.495	0.664±0.521	94.3%	93.6%	100.0%	99.2%	100.0%	97.3%
2	0.493±0.188	0.565±0.238	98.5%	98.0%	100.0%	98.8%	100.0%	97.5%
3	0.747±0.478	0.760±0.718	97.3%	97.0%	100.0%	91.6%	99.8%	71.4%
4	0.634±0.577	0.773±0.586	95.2%	91.0%	99.8%	94.6%	99.1%	83.0%
5	0.736±0.481	1.072±1.229	96.0%	93.1%	99.9%	94.2%	99.9%	76.0%
6	0.529±0.436	0.498±0.272	95.7%	96.2%	100.0%	92.9%	99.6%	56.9%
7	0.786±0.514	0.789±0.639	96.7%	93.4%	99.7%	92.0%	98.5%	67.7%
8	0.734±0.396	0.766±0.476	95.2%	94.1%	99.7%	96.0%	98.1%	58.9%
9	0.452±0.256	0.532±0.478	94.6%	92.8%	100.0%	96.1%	100.0%	82.1%
10	0.565±0.272	0.671±0.565	96.8%	93.9%	99.9%	96.4%	99.9%	70.8%
All	0.633±0.436	0.700±0.611	96.2%	94.5%	99.9%	95.3%	99.4%	76.2%

NOTE. MAE, Mean Absolute Error; CC, Correlation Coefficient; ETLD, Enhanced Tracking-Learning-Detection Framework; OTLD, Original Tracking-Learning-Detection Framework.